Published in: Materials Science and Technology 25 (2009) 687-698

Using differential scanning calorimetry as an analytical tool for ultrafine-grained metals processed by severe plastic deformation

Nong Gao[1,*], Marco J. Starink[1] and Terence G. Langdon[1,2]

[1]Materials Research Group, School of Engineering Sciences
University of Southampton, Southampton SO17 1BJ, U.K.
[2]Departments of Aerospace & Mechanical Engineering and Materials Science
University of Southern California, Los Angeles, CA 90089-1453, U.S.A.

Abstract

Differential Scanning Calorimetry (DSC) is a thermal analysis technique that measures the energy absorbed or released by a sample as a function of temperature or time. Analysis by DSC has wide applications for examining solid-state reactions and solid-liquid reactions in many different materials. Quantitative analyses of the kinetics of reactions may be assessed by reviewing the interrelation between activation energy analysis methods. In recent years, DSC has been applied in the examination and analysis of bulk ultrafine-grained materials processed through the application of Severe Plastic Deformation (SPD). This overview examines these recent reports with reference to materials processed using the procedures of Equal-Channel Angular Pressing (ECAP), High-Pressure Torsion (HPT) and Accumulative Roll-Bonding (ARB). In addition, some critical issues related to DSC analysis are also discussed.

Keywords: Accumulative Roll-Bonding (ARB), Differential scanning calorimetry (DSC), Equal-Channel Angular Pressing (ECAP), High-Pressure Torsion (HPT), Severe Plastic Deformation (SPD).

[*]Contributing author: Nong Gao (n.gao@soton.ac.uk)

Introduction

Calorimetry is one of a number of analytical techniques which are known collectively as thermal analysis methods. Differential Scanning Calorimetry (DSC) is a thermal analysis procedure that is designed to measure the energy absorbed or emitted by a sample as a function of temperature or time.[1,2,3,4] In this context, the term "differential" denotes measurements that involve a determination of the relative behaviour of a selected substance with respect to a reference material. When a thermal transition occurs in the sample, DSC provides a direct calorimetric measurement of the enthalpy change at the reaction temperature.

Measurements by DSC have been applied extensively for the analysis of a wide range of materials, including in the analysis of various solid-state reactions such as precipitation, homogenisation, devitrification and recrystallisation and in the analysis of solid-liquid reactions such as incipient melting and solidification. The principles of DSC have been used also in attempts to measure the volume fractions of phases present in light alloys.[4] There are several specific advantages in using DSC analysis and these include the rapid analysis time (typically 0.1 to 1 h); the very small sample size (typically ~1-20 mg); the relatively easy characterization of thermal transitions and the ability to track material changes as a function of time and temperature. The simplicity of the DSC technique, combined with the general availability of the required apparatus, make it an economical method for determining the temperatures of solid-state reactions. Furthermore, the methods of quantifying the measurements of thermal energy (enthalpy changes) lead to an improved knowledge of the chemical and microstructural changes occurring within the selected material and therefore they assist in optimising the processing route.[5,6,7]

Many different techniques have been developed over the last two decades involving the processing of materials through the application of severe plastic deformation (SPD). Specifically, SPD processing has been defined formally as "any method of metal forming under an extensive hydrostatic pressure that may be used to impose a very high strain on a bulk solid without the introduction of any significant change in the overall dimensions of the sample and having the ability to produce exceptional grain refinement."[8] Thus, processing by SPD leads to very small grain sizes and the processed metals are usually termed ultrafine-grained (UFG) materials where the average grain sizes are typically less than ~1 μm and lie either within the submicrometer range of 100 nm – 1.0 μm or the nanometer range of <100 nm.

Although several different SPD processing techniques are now available, most attention has been devoted to the processing of metals using equal-channel angular pressing (ECAP),[9,10,11,12] high-pressure torsion (HPT)[13,14] or accumulative roll-bonding (ARB).[15,16] Depending upon the crystal structure, the processed microstructures produced by these procedures generally have grain sizes lying within the range of ~70–500 nm. Experiments have shown that UFG metals and alloys processed by SPD techniques have superior mechanical properties such as high strength with good ductility and, provided the microstructures are reasonably stable at elevated temperatures, excellent superplastic forming capabilities at relatively low temperatures and high strain rates.[17,18,19,20]

To date, many different analytical techniques have been employed in analyzing SPD-processed materials, including transmission electron microscopy (TEM), scanning electron microscopy (SEM), electron back-scatter diffraction (EBSD) and orientation imaging microscopy (OIM). Nevertheless, due to its high speed, convenience, accuracy and versatility, DSC analysis is now becoming increasingly

attractive as an analytical tool for studying microstuctural evolution and the parameters affecting the physical and mechanical characteristics of materials processed using SPD techniques. Accordingly, the objective of this report is to provide an overview of the latest developments in the application of DSC to materials processed using different SPD methods. The basic principles of DSC are presented in the following section, the subsequent section introduces the application of DSC to commercial materials and light alloys and the next section summarizes recent applications of DSC to SPD materials processed using ECAP, HPT and ARB. Finally, the concluding section outlines some important issues that should be considered in conducting an accurate analysis of DSC data.

The working principles of DSC

The fundamental principle of using DSC as a thermo-analytical tool is the requirement to measure, as a function of temperature, the difference in heat that is required to increase the temperature of a sample with respect to a reference material.[4] In general, both the sample and reference are maintained at approximately the same temperature throughout the experiment and a temperature programme is established so that the temperature of the sample increases linearly with time. Thus, if the sample undergoes a physical transformation during heating, such as a phase transition, precipitation or recrystallisation, a heat flow or local heat input is established to maintain both the sample and the reference material at the same, or nearly the same, temperature.[4] For example, a solid sample melting to a liquid requires more heat flow to the sample than a sample undergoing crystallization because the sample will absorb heat as it undergoes the endothermic phase transition from a solid to a liquid.

There are two basic types of DSC, termed heat flux DSC and power compensation DSC,[21] and Fig. 1 shows a schematic cross-section of these two types.[4] In heat flux DSC shown in Fig. 1*a*, a single furnace is employed and the signal derives directly from the difference in temperature between the sample and the reference material. For this situation the DSC cell contains two pans in which one pan is used to heat a reference and the other pan is used to heat the sample.[22] The calibration of heat flux DSC is performed by using materials for which the heat evolution is already well known.[23] In most cases, pure In and pure Zn are used. By contrast, two furnaces are used for power compensation DSC, as depicted schematically in Fig. 1*b*, and the signal is related to the differential heat that is needed to keep the sample and the reference at the same temperature. For both types of DSC, the sample is generally in the form of a disc having a thickness of about 0.5 to 2.0 mm and a diameter of about 5.0 to 8.0 mm.[24] These two types of instrument are fundamentally different and many researchers consider that only a power compensation DSC represents a true DSC instrument whereas heat flux DSC corresponds essentially to a calibrated differential thermal analyser (DTA). In practice, the term DSC is generally used to describe both types of instrument.

Several procedures are usually conducted in order to isolate the true heat effects due to reactions in the sample from any potential spurious effects related to the equipment and its environment.[4] Two separate DSC runs are usually conducted under identical conditions. In analysing aluminium alloys, for example, high purity annealed aluminium discs are placed in both the sample and the reference pan in the first run. During the second run, the pure aluminium disc remains in the reference pan but a new disc of the selected alloy is placed in the sample pan.[25] By subtracting the results

obtained in the second run from those measured in the first run, it is possible to obtain a correction for any spurious effects related to the equipment and environment.

As an example, Fig. 2 shows a corrected thermogram obtained during the heating of an A1-1.18% Cu-0.51% Mg-0.21% Mn alloy aged at 150°C and undergoing a DSC scan using a temperature rise of 10°C/min.[26] Thus, the peaks and troughs in the recorded curves, corresponding to S formation and the dissolution of co-clusters and S dissolution, respectively, demonstrate the occurrence of various precipitation and dissolution processes.

The application of DSC to commercial materials and light alloys

Applications for commercial materials

The DSC technique has been proven as a very useful and reproducible technique for investigating various characteristics of commercial materials.[1,2,3,4] By using DSC, it is possible to observe and study fusion, crystallization, glass transition temperatures, oxidation, the principles of phase diagrams and other various chemical reactions. For example, DSC has been widely used in the polymer industry where it is an effective tool for studying curing processes and thereby optimising the polymer properties. It is well known that thermal analysis is an important analytical tool within the pharmaceutical industry and in this respect DSC curves provide a useful opportunity for accurately measuring drug purities. This is because the temperature range associated with the melting of a mixture of compounds depends upon their relative amounts such that compounds having lower purities exhibit both a broadened melting peak and an onset at a lower temperature by comparison with a pure compound. All transitions in materials involve heat flow, either into the sample during an endothermic event or out of the sample during an exothermic event, and in practice

DSC may be employed as the ideal and universal detector for measurements of a wide range of transitions in pharmaceutical materials. Analysis by DSC is used also in food science research. For example it may be employed to determine water dynamics in which changes in the water distribution may be correlated directly with changes in the texture. In addition, DSC is used frequently as an analytical tool in the field of oils and fats.[27]

Applications for light alloys

In the conventional processing of light alloys, as in extrusion and casting, there may be many different thermomechanical processing steps and each step should be controlled within a narrow processing range in order to attain the required properties. In the absence of DSC, any determination of the optimum processing conditions for each thermomechanical step is clearly time and labour intensive. These limitations may be removed by using DSC to determine reaction temperatures and reaction rates of microstructural changes with a high degree of sensitivity and reproducibility. Thus, DSC is an excellent tool for ensuring quality control, process optimisation and appropriate alloy development.[4,22]

The DSC analysis of a sample, obtained during heating at a selected heating rate, provides information on the temperature ranges for the different reactions in addition to yielding the typical thermal peaks which are characteristics of reactions occurring in the light alloys. The high degree of reproducibility in DSC analysis provides critical information on the metallurgical state of the alloy which may be used for quality control during the production processing. For example, the presence of any incipient melting phase is undesirable in light alloys because it may lead to cracking of the ingot during hot rolling. By selecting suitable DSC experiments, it is

possible to determine homogenisation conditions which will eliminate the melting in the homogenised alloy. The choice of the heat treatment conditions, such as the solution temperature and quenching rates, may change the occurrence of precipitation and dissolution in the alloys even when the conditions are changed by only small amounts. Nevertheless, DSC analysis is very sensitive to these reactions and the use of DSC provides an opportunity to detect and avoid these problems. It is important to note also that one increasingly important application of DSC/DTA is in the determination of solid fraction curves for metals as they are processed in their semi-solid state.[28]

The precipitation of metastable precursors of soluble equilibrium phases causes precipitation strengthening in heat-treatable alloys.[4] The arrangements of peaks in the DSC curve demonstrate the particular sequence for any selected alloy and this information on the different stages of precipitation may be used effectively in process development. It is feasible in practice to link the different precipitates with the DSC peaks and age hardening curves. [4] Furthermore, the effect of alloying elements on the precipitation process may be examined with DSC because the procedure is effective in resolving changes in heat effects due to small changes in composition that are generally difficult to distinguish using other techniques.

DSC can be used also to obtain the effective activation energies of thermally-activated reactions. [4]

The volume fractions of precipitation phases in light alloys have a strong influence on fundamental material properties such as the yield strength, rate of work hardening and toughness. A method has been developed for obtaining the volume fractions of the precipitates based on the heat evolutions due to precipitation of the

phases as measured by DSC.[4,29,30,31,32] Assuming that a precipitate of composition $M_mA_aB_bC_c$ is formed, the heat effect measured in DSC is then given by:

$$\Delta Q_{\mathrm{MmAaBbCc}} = \Delta x_{\mathrm{MmAaBbCc}} \Delta H_{\mathrm{MmAaBbCc}} \qquad (2)$$

where ΔQ is the heat effect in DSC, Δx is the amount of phase formed and ΔH is the enthalpy of formation of that phase. Equation (2) is valid also for dissolution reactions where the process is endothermic and ΔQ and Δx are negative quantities.[4]

The use of DSC for ultrafine-grained materials processed by SPD

Interest in the processing of bulk UFG materials through the application of SPD methods has grown rapidly over the last decade.[8] All of these procedures are capable of introducing large plastic straining and significant microstructural refinement in bulk materials. Thus, techniques such as ECAP, HPT and ARB are now well-established for the processing of bulk UFG materials. There are also some other SPD techniques under current development but they have received only limited attention to date.[8] Although the application of DSC to SPD materials has increased recently, there is little systematic study of the thermal stability of UFG materials processed by SPD.[33] However, investigations of the thermal stability of SPD-processed materials is important because these materials not only have very small grain sizes but also, depending upon the specific alloys and processing conditions, they may have high dislocation densities, high vacancy concentrations and high internal stresses. As a result, the ultrafine microstructures are often inherently thermally unstable. Since the energy released in DSC analysis is directly related to microstructural changes, such as changes in the dislocation densities and the occurrence of grain growth, DSC analysis is an especially effective tool for studying

the thermal stability of UFG materials. This section describes some examples of recent DSC applications using SPD-processed materials

Applications using ECAP

Copper

There are several reports related to the DSC analysis of copper materials processed by ECAP.[34,35,36,37] The thermal stability of pure copper specimens deformed by ECAP for up to eight passes was examined by DSC using scan temperatures from 300 to 750 K and a heating rate of 40°C/min.[36] As illustrated in Fig. 3, a broad exothermic peak was observed in the DSC curves for each sample.[36] It was found that the temperature of the DSC peak, which relates to the recovery of the microstructure, decreased with increasing strain. In addition, the heat released in the DSC curves increased with increasing strain up to a strain of ~4. These changes were explained in terms of an increase of the stored energy introduced by SPD which raised the driving force for nucleation of new strain-free grains so that nucleation was then achieved at lower temperatures.

Measurements by DSC were performed for Cu rods deformed by ECAP up to shear strains of ~5 while applying three different deformation paths, A, B_C and C, over temperatures from 40 to 600 °C using a heating rate of 10°C /min:[37] In experiments in ECAP, processing routes A, B_C and C refer to pressing in consecutive passes through the ECAP die either without rotation of the specimen about the longitudinal axis or with rotations of 90° in the same sense or 180° between each pass, respectively.[38] Using the following relationship, the stored energy of the dislocations may be related to their density, *N*, as follows:[39]

$$E_{stor} = Gb^2 \frac{N}{4\pi k} \ln\left(\left(b\sqrt{N}\right)^{-1}\right) \qquad (3)$$

where G is the shear modulus, b is the absolute value of the Burger vector and κ represents the arithmetic average of 1 and $(1-\nu)$ with the Poisson ratio ν taken as 0.343 assuming equal parts of edge and screw dislocations. The vacancy concentration may be estimated from the stored energy of the vacancies divided by the formation energy $\Delta H_V^f = 1.217eV$ per vacancy.[40]

Figure 4 shows the stored energy plotted against the shear strain, γ, as determined by DSC at different shear strains and using the three different processing routes.[37] It was found that the stored energy increased almost linearly with increasing number of passes for routes A and B_c although some discontinuities were visible when using route C. Figure 5 shows the evaluated vacancy concentrations determined from the results of DSC and the residual electrical resistometry (RER) as functions of the shear strain for processing routes A, B_C and C, where the dashed-dotted line indicates the evolution of the vacancy concentration after conventional cold working.[41] In general, there is a steady increase in the vacancy concentration with increasing amounts of deformation but for route C the results are slightly different because there are higher values of the stored energy and resistivity after two passes which demonstrate an enhanced vacancy concentration at these early stages. This is consistent with the principles of route C when it is recognised that this is a redundant strain process where the deformation is reversed in every other ECAP pass.[38] It is important to note that Fig. 5 demonstrates an excellent agreement between the DSC measurements and the resistometric data.

Aluminium

There are more reports of DSC analysis related to aluminium alloys processed by ECAP.[42,43,44,45] The precipitation and evolution of microstructure in a commercial

wrought Al-2024 (Al-4.4% Cu-1.5% Mg-0.6% Mn) alloy and a spray-cast Al-7034 (Al-11.5% Zn-2.5% Mg-0.9% Cu-0.2% Zr) alloy were studied by DSC after processing by ECAP.[46,47,48] Figure 6 shows that there are many similarities in the DSC curves for Al-2024 samples either annealed or processed by ECAP through different numbers of passes but these curves are significantly different from the curve obtained for the same alloy in the T351 condition.[47] A DSC analysis of the T351 sample shows there are three thermal reactions in the DSC curve and these are identified specifically as co-cluster dissolution (160-240°C) (I), S formation in the range of 240-300°C (II) and S dissolution in the range of 300-500°C (IV).[26] The small peaks occurring at about 380°C (III) were recorded for all ECAP samples but not for the T351 and annealed samples and it is apparent that these peaks shift slightly to higher temperatures with increasing numbers of ECAP passes. The heat contents of these exothermic effects decrease slightly at 4, 6 and 8 passes by comparison with 2 passes of ECAP. Metallographic examination demonstrated that the small exothermic peak around 380°C was due to recrystallisation. A refinement of the particles in this alloy that are in the size range of about 50 to 2000 nm, such as Al_7Cu_2Fe and $Al_{20}Cu_2Mn_3$,[49] enhances their effectiveness as recrystallisation inhibitors and this provides an explanation for the increase in the recrystallisation temperature with increasing number of ECAP passes.

Figure 7 shows there are six thermal reactions in the DSC curves for the Al-7034 alloy which was subjected to ECAP using route Bc performed at 200ºC.[47] They are interpreted as Guinier-Preston (GP) zone and/or η′-phase dissolution (I), formation of the η-phase (II), coarsening of the η precipitates (III), dissolution of the η-phase (IV), incipient melting of the T-phase (V) and the onset of full melting of the alloy (VI) [48]. The drastic changes occurring in the first pass of ECAP show the

influence of the exposure to temperature at 200ºC during ECAP combined with the pronounced effect of SPD on the microstructure In this example, extensive η-phase formation occurs which eliminates the Guinier-Preston (GP) zones and η′-phase reactions in the DSC experiment. The breaking of the rod-like $MgZn_2$ precipitates which pre-exisit in the alloy before ECAP was shown by TEM to occur primarily in the first pass of ECAP.[50,51]

An investigation was conducted in which DSC was used to evaluate the microstructural evolution occurring in ECAP-processed plus naturally-aged UFG and coarse-grained (CG) Al-7075 alloys (Al-5.60% Zn-2.50% Mg-1.60% Cu-0.50% Fe-0.40% Si-0.30% Mn-0.23% Cr-0.20% Ti) under a constant heating rate of 5 or 10 °C/min.[43] The ECAP sample was processed for two passes using route B_c. Figure 8 shows that both UFG and CG samples have an endothermic reaction at lower temperatures (region I), exothermic reactions at intermediate temperatures (region II) and an endothermic reaction at higher temperatures (region III).[43] With an increase in the heating rate from 5 to 10°C/min, all reaction regions are shifted towards higher temperatures. The regions labelled I and III were interpreted as due to the dissolution of the Guinier-Preston (G–P) zones and the dissolution of the equilibrium hexagonal η phase, respectively, and region II includes the intermediate metastable phase η′ (IIA) and formation of the equilibrium η phase (IIB).[43] It is important to note that the DSC graphs in this investigation appear to have a very low enthalpy of dissolution of the η phase by comparison with previous work on similar Al-Zn-Mg alloys.[52,53,54] Since SPD should have no significant effect on these high temperature reactions, this may be due to the use of an inaccurate baseline at higher temperatures. However, there are some significant differences in the DSC curves between the UFG and CG samples. Thus, region I of the CG sample is broader and the peak temperature is lower than for

the UFG sample. The two exothermic peaks of the CG sample in region II have more overlapping than for the UFG sample. In addition, the first exothermic peak temperature (IIA) of the UFG sample is about 20°C lower than for the CG sample. The reaction enthalpies, ΔH, may be obtained by integrating the areas of the reaction peaks. As shown in Table 1, ΔH of the UFG sample is equivalent or similar to that of the CG sample for regions I and III but ΔH of the UFG sample is larger than for the CG sample in region II. Therefore, the DSC analysis shows that processing by ECAP accelerates the phase precipitations but without affecting the sequence of the precipitations.

An analysis by DSC was conducted using a heating rate of 20°C/min to evaluate the ageing behaviour and thermal stability of Al-Mg-Si (Al-0.34% Mg-0.51% Si-0.16% Fe-0.014% Mn-0.10% Zr) and Al-Mg-Si-Sc (Al-0.36% Mg-0.50% Si-0.14% Fe-0.013% Mn-0.10% Zr-0.12% Sc) alloys processed by ECAP.[44,55] The DSC thermograms in Figure 9 indicate the precipitation sequence and kinetics are similar for these two alloys.[43] The first exothermic peak at about 280°C for the solution annealed alloys represents two partially superimposed formation peaks of the β'' and β' metastable phases and the exothermic peak at about 430°C is due to the formation of the equilibrium β-Mg_2Si phase. The only difference is that the ECAP scandium-free samples shown in Fig. 9*a* exhibit a clear recrystallisation peak at a temperature in the range of 315-360°C whereas the alloy containing scandium shown in Fig. 9*b* exhibits no such peak. Apparently, the Sc addition suppresses recrystallisation and thus the UFG structure is retained to temperatures exceeding 450°C as proven by TEM examination.[44] It appears that processing by SPD induces changes in the precipitation kinetics, probably by increasing both the effective diffusivity in the lattice and the density of nucleation sites for precipitation, and this

effect is confirmed in Fig. 9*a* by noting there is a shift in the recrystallisation peaks towards lower temperatures when the number of ECAP passes is increased.

The results of DSC analyses on an Al-3% Mg alloy after ECAP, after cold-rolling, and after cold-rolling and subsequent annealing are shown in Fig. 10.[56] From these DSC curves, it was found that ECAP and cold-rolled samples exhibit a significant heat release whereas there is no heat effect in the fully-annealed condition. The results show there are two peaks in the DSC curve after ECAP which, as demonstrated by TEM observations,[56] are associated with the advent and completion of the recrystallisation. By contrast, there is only a single peak in the cold-rolled condition which is related to the advent of recrystallisation.[57,58]

Magnesium

Analysis by DSC was used to study the effect of the ECAP temperature on the microstructure of the magnesium alloy AM60 (Mg–6% Al–0.13% Mn) using three samples pressed through a total of 10 passes at 150, 210 and 350°C.[59] The results are shown in Fig. 11 where four peaks are visible in the DSC curves of the ECAP samples. The first peak occurs around 150°C, the second peak occurs around 300°C and is present only in the ECAP samples and not in the as-received cast alloy, the third peak occurs at 390°C for the as-received alloy and moves to lower temperatures from 385 to 360°C with decreasing ECAP temperature and the fourth peak appears at about 430°C for all samples. In order to interpret these DSC results, extensive TEM was conducted for a series of samples which were heated to selected temperatures of 100, 230, 330 or 400°C and subsequently quenched to room temperature. The first peak was attributed to the annealing of vacancies which arise either from quenching or from the ECAP processing[37]. The second peak was mainly due to a rearrangement of the ECAP-induced dislocations. The third peak was associated with the dissolution

of the $Al_{12}Mg_{17}$ precipitates plus the annealing dislocations where the shift of this peak to lower temperatures in the ECAP samples was attributed to the presence of ECAP-induced dislocations and extensive vacancy clusters.

Other materials

The effect of high temperature ECAP on the transformation behaviour of the Ti–50.3 at.% Ni shape memory alloy was studied extensively by DSC.[60] Figure 12*a* shows the DSC curve for the alloy before ECAP where there are two exothermic peaks on cooling associated with the transformation of the B2 parent phase to the R-phase and then to the martensitic phase transformations.[61] By contrast, only one endothermic peak is observed on heating which suggest a reverse R-phase transformation and a reverse martensitic transformation overlap.[62] Figure 12*b* shows the DSC curves of the specimen after two passes of ECAP at the high temperature of 823 K.[60] It was found there was only one broadened exothermic peak on the cooling curve and the B2 to R-phase transformation peak was not clearly defined but, at the same time, the transformation temperatures decreased sharply. These results confirm that processing of TiNi by SPD in high temperature ECAP affects the microstructural evolution in the alloy.

The morphological changes of isotactic polypropylene (iPP) subjected to varying shear strains by ECAP was studied by X-ray diffraction and DSC.[63] The enthalpy of fusion, ΔH, was calculated by integrating the area under the baseline-corrected thermogram between 130 and 175°C and the percentage crystallinity was estimated from the ratio $\Delta H/\Delta H_0^{iPP}$ where ΔH_0^{iPP} for 100% iPP was taken as 148 J/g.[64,65] Figure 13 shows that both the crystallinities measured by DSC (χ_{DSC}) and by X-ray decrease with increasing shear strain.[63] The difference in the values of the

crystallinities between X-ray and DSC was explained on the basis of the ΔH_0^{iPP} value used to calculate the crystallinity from DSC which varied in the range of 138-168 J/g. An investigation was conducted of microstructural evolution in a highly-textured semicrystalline polyethylene terephthalate (PET) processed by ECAP by making use of small-angle X-ray scattering, TEM and DSC.[66] The DSC analyses demonstrated that the melting enthalpy, ΔH, of PET increased with increasing shear strain and the increase was explained in terms either of an increase in the crystallinity through stress-induced crystallization or to a squeezing of the crystalline phase within the overall structure.[67]

Applications using HPT

The processing of UFG bulk solids by HPT is an especially attractive procedure because, by comparison with ECAP, it leads both to smaller grain sizes and to a higher fraction of high-angle grain boundaries.[68,69] However, to date there are only a limited number of reports describing the application of DSC to materials processed by HPT.

Figure 14 shows the DSC curves of copper alloy samples (98.51 % Cu-1.49% Si) processed by HPT through various numbers of torsional turns.[33] Two exothermic peaks are evident in each curve and the first peak at lower temperatures in the range of 180–280°C was due to recrystallisation. In order to identify the origin of the second peak, DSC runs were conducted on a coarse-grained as-received sample and this result, shown in Fig. 14*b*, depicts an exothermic reaction which matches the second exothermic peak. It was accordingly deduced that the second peak was caused by oxidation of the copper alloy. Figure 15 shows the energy release calculated from the first peak for samples processed by HPT through different numbers of turns equivalent to different imposed strains.[33] The result indicates that the energy release

increases and the peak position shifts to lower temperature with increasing turns in HPT.

Nickel rods of 99.99% and 99.998% purity were deformed by HTP under different applied pressures from 1 to 8 GPa and using different levels of shear strain from 1 to 25.[70] An analysis by DSC showed it was feasible to detect differences in the thermal effects even when there were only very small compositional changes between the two materials. Thus, the higher purity 99.998% Ni exhibited two exothermic peaks in the DSC curve as shown in Fig. 16*a* whereas the lower purity 99.99% Ni revealed only one peak at the higher temperatures as shown in Fig. 16*b*.[70] Based on an analysis of residual electrical resistivity and activation enthalpies, the two exothermic peaks were attributed to the annealing of single and/or double vacancies and dislocations, respectively. Therefore, the peaks occurring at the low and high temperatures were designated the 'vacancy peak' and the 'dislocation peak', respectively. Figure 17*a* shows that the dislocation peak shifts to lower temperatures with increasing strain whereas the vacancy peak remains at almost a constant temperature. It is also apparent that the 99.99% Ni shows higher dislocation peak temperatures compared with the 99.998% Ni and this was attributed to a decreased dislocation mobility in the lower purity Ni because of the interactions with impurity atoms. Figure 17*b* demonstrates the change in the stored energies calculated from the DSC results for the two purities of nickel, where both samples show an increase in the dislocation stored energy with increasing shear strain.[70]

Samples of hydrogen-free pure 99.95% Pd were processed by HPT and then analyzed by DSC and the results were compared with hydrogenated and HPT-processed samples.[71] Under hydrogen-free condition, the HPT Pd samples showed two exothermic peaks where the first peak appeared at about 373 K and arose from

the annealing of single and/or double vacancies and the second was a double peak occurring between 523 and 553 K which was identified with the annealing of both vacancy clusters and dislocations.[72,73] Figure 18 shows a comparison of the DSC analysis of hydrogenated plus HPT-processed Pd (dashed line) and unprocessed but hydrogenated Pd (solid line) and these results demonstrate that desorption of hydrogen in the HPT sample occurs at a temperature which is about 35ºC lower by comparison with the unprocessed sample.[71] The DSC results indicate that hydrogenation plus HPT processing leads to a very high concentration of deformation-induced vacancies where this concentration is more than an order magnitude higher than without hydrogenation.

Straining by high pressure torsion was applied to $Al_{90}Fe_5Nd_5$ powders to achieve cold consolidation into bulk nanostructured discs under an applied pressure of 5 GPa.[74] Figure 19*a* shows the DSC curve of melt-spun amorphous $Al_{90}Fe_5Nd_5$ before applying HPT and Fig. 19*b* shows the DSC curves of the $Al_{90}Fe_5Nd_5$ powder after processing by HPT.[74] Although information on the heating rate was not included in this report, it is apparent there are three exothermic peaks prior to HPT including a broad peak between 150 and 270 °C, a sharp large peak around 350°C and a weaker peak around 570 °C. The first exothermic peak between 150 and 270°C in Fig. 19*a* was attributed to precipitation of fcc-Al in the amorphous matrix but it is apparent from Fig. 19*b* that this peak disappears after processing by HPT. Apparently HPT induces crystallisation in these amorphous materials.

Applications using ARB

The accumulative roll-bonding (ARB) process produces not only UFG structures in bulk solids but also it leads to specific deformation textures in various

materials.[75,76] However, very little work has been performed to date to apply DSC analysis to materials processed by ARB.

Figure 20*a* shows the DSC curves of 99.99% purity copper processed by ARB through various numbers of cycles.[75] It was found in this investigation that exothermic peaks appeared at 210-253°C after the ARB processing and subsequent observations of the microstructures by EBSD and TEM, using samples before and after the DSC measurements, demonstrated these peaks were caused by primary recrystallisation. It is apparent that the positions of the peaks shift to lower temperatures with increasing numbers of cycles and the temperatures of the peaks are similar to those recorded for copper processed by HTP.[33] These results indicate that an increase in the numbers of cycles in ARB enhances the occurrence of recrystallisation at lower temperature. Figure 19*b* shows the stored energy estimated from the DSC curves and the Vickers hardness, *HV*.[75] This plot demonstrates that the stored energy is in the range of ~43-53 J/mol and the Vickers hardness has a similar tendency to the stored energy whereby it increases with increasing numbers of ARB cycles.

Important issues related to DSC analysis

Although there are many advantages in applying DSC analysis, it is important to recognise that the use of DSC has particular drawbacks and difficulties that are associated specifically with the characteristics of the experimental methodology. Several factors affect the accuracy of the DSC results including sample preparation, testing conditions and the baseline correction.[4,77]

Sample preparation and testing conditions

Sample preparation for a DSC study of a bulk material is a relatively simple process. Suitable disc-shaped samples are readily obtained by slicing machined

cylinders, normally 5 to 8 mm in diameter, to provide discs having thicknesses of about 0.5 to 2 mm. If the material is in the form of powder or ribbons, the sample may be put directly into a crucible or sealed pan.[4] In practice, the effects of sample preparation are often not significant in DSC analysis. Nevertheless, procedures such as punching, severe machining and/or cutting may introduce deformation in soft light alloys and this may influence the advent of precipitation in heat-treatable aluminium-based alloys because it will provide favourable sites for heterogeneous nucleation and may lead to an annihilation of quenched-in excess vacancies.[4,78,79] For example, the deformation introduced by the punching of disc samples had a significant impact on the response in the DSC curves for an Al-6061 alloy and, as a result, clustering was suppressed at low temperatures and the precipitation and dissolution of the equilibrium β-Mg_2Si phase was accelerated.[80] On the other hand, treatments at relatively high temperatures may cause oxidation and surface reactions which could lead to a loss of alloying elements to the atmosphere thereby affecting the final results of the DSC analysis.[4]

When using DSC to determine transition temperatures and the enthalpy of an alloy, it is necessary to choose appropriate heating and cooling rates.[7] Any calibration of the instrument is only valid for the particular heating rate at which it was conducted because the sensors in any DSC are at some distance from the sample so that there may be a thermal gradient between the sample and the sensor. By using different heating rates, different transition temperatures may be obtained. In practice, however, the common heating rates are 10-40°C/min as this leads to a good resolution and at the same time avoids the introduction of unwanted noise.

The baseline correction

In analysing linear heating experiments, the baseline of the DSC needs to be carefully considered because these baselines are dependent upon temperature and they gradually shift over time.[4,81] In DSC curves, a baseline drift may result from thermal imbalances between the sample and the reference of the calorimeter, thereby introducing slight changes in the baseline position during the course of a single experiment. Solid-state reactions in metals and alloys, such as precipitation, recovery and recrystallisation, normally cause relatively small heat effects and therefore the baseline correction procedures are critical and accordingly the baselines must be checked regularly. On the other hand, solid-liquid and liquid-solid reactions generally produce much larger heat flows and the baseline correction is then less important or, under some conditions, may even be omitted. [4]

A baseline run should be conducted at the same heating rate used for the DSC experiment and with a real sample, where this run is conducted either just before or just after the DSC experiment. The required frequency of baseline runs is determined by the time dependency of the baseline. In the DSC analysis of Figs. 6 and 7, all of the DSC runs were corrected by subtracting the DSC baseline obtained from a run with an empty pan. For additional baseline corrections, and in order to compensate for heat capacity differences and baseline drifts, a second-order polynomial function may be subtracted from the measured heat flows.[4] A review of the extensive literature on DSC analysis shows there are many publications in which DSC curves are presented without providing any explicit indication of the position of the baseline. Although such work may provide some useful qualitative information, in practice it is not suitable for any detailed quantitative or even semi-quantitative analysis of the enthalpy changes.

Assistance with other analytical techniques

An analysis by DSC is a very valuable and efficient tool for determining the different reactions occurring in various materials and light alloys. However, before applying DSC it is important to consider the reactions that will probably occur during a calorimetric experiment and thereby to estimate the nature of any phases that may evolve. An important issue is that a calorimetry experiment cannot identify, *a priori*, the individual phases involved in the reactions. Therefore, other techniques, such as electron microscopy and electron diffraction, are a necessary prerequisite in identifying these reactions and phases.[4] Most conclusions from DSC analysis are dependent either upon references to earlier data on the same or similar materials or upon supplementary data obtained on the same material through the use of additional analytical techniques.

In order to identify the phase changes in DSC curves more effectively, it is useful to use three samples and to check the data using other techniques. Thus, the first sample may be heat-treated to a condition corresponding to the onset of the thermal effect, the second sample may be heat-treated to a condition corresponding to the end of the thermal effect and the third sample may be heat-treated to some intermediate stage. In this procedure, all three samples are rapidly quenched when the heat treatments are completed and the samples are then examined using an analysis technique that provides conclusive and unambiguous information on the phases involved in the reactions. These procedures were outlined and several examples were reviewed earlier.[4]

Conclusions

Thermal analysis by DSC is an experimental tool that measures the energy absorbed or emitted by a sample as a function of temperature or time. The DSC technique may be widely used to obtain qualitative information on the state of the

microstructure and the precipitation sequence. The simplicity and rapid nature of the DSC technique, together with the general availability of the DSC apparatus, make it an economical method for obtaining the temperatures of reactions.

In broad terms, DSC has broad applications for the analysis of solid-state reactions and solid-liquid reactions in many different materials but in recent years it has been applied increasingly for the analysis of bulk ultrafine-grained materials processed through the application of severe plastic deformation. This overview provides a summary of the more important contributions in this important area and discusses some of the issues that require consideration in interpreting the results of any DSC analysis.

In summary, DSC is a very useful and powerful analytical tool for effectively investigating microstuctural evolution and the influence of SPD parameters on the processed materials.

Acknowledgements

The work was funded in part by EPSRC under Grant No. EP/D00313X/1.

References

1. J. A. Dean: 'The Analytical Chemistry Handbook', 15.1–15.5; 1995, New York. McGraw Hill.

2. E. Pungor: 'A Practical Guide to Instrumental Analysis', 181–191; 1995, CRC Press, Boca Raton, Florida.

3. D. A. Skoog, F. J. Holler and T.A. Nieman: 'Principles of Instrumental Analysis', 5th edn, 905–908; 1998, Saunders, Philadelphia, PA, USA.

4. M. J. Starink: *Intl Mater. Rev.*, 2004, **49,** 191-226.

5. D. L. Sponseller: 'Superalloys 1996, Proceedings of the Eighth International Symposium on Superalloys," (Ed. R.D. Kissinger, D.J. Deye, D.L. Anton, A.D. Cetel, M.V. Nathal, T.M. Pollock and D.A. Woodford), 1996, 259-270, TMS, Warrendale, PA, USA.

6. S. W. Chen and S. C. Jeng: *Metall. Mater. Trans*., 1997, **A28**, 503-504.

7. L. A. Chapman: *J. Mater. Sci.*, 2004, **39**, 7229-7236.

8. R. Z. Valiev, Y. Estrin, Z. Horita, T. G. Langdon, M. J. Zehetbauer and Y. T Zhu: *JOM*, 2006, **58** (4), 33-39.

9. V. M. Segal, V. I. Reznikov, A. E. Drobyshevskiy and V. I. Kopylov: *Russian Metall*, 1981, **1**, 115-123.

10. R.Z. Valiev, N.A. Krasilnikov and N. K. Tsenev: *Mater. Sci. Eng.,* 1991, **A137,** 35-40.

11. V. M. Segal: *Mater. Sci. Eng*., 1995, **A197**, 157-164.

12. R. Z. Valiev and T. G. Langdon: *Prog. Mater. Sci.*, 2006**, 51**, 881-981.

13. N.A. Smirnova, V. I. Levit, V. I. Pilyugin, R. I. Kuznetsov, L. S. Davydova and V. A. Sazonova: *Fiz. Metal. Metalloved*, 1986, **61**, 1170-1177.

14. A. P. Zhilyaev and T. G. Langdon: *Prog. Mater. Sci.*, 2008, **53**, 893-979.

15. Y. Saito, N. Tsuji, H. Utsunomiya, T. Sakai and R. G. Hong: *Scripta Mater.*, 1998, **39**, 1221-1227.

16. Y. Saito, H. Utsunomiya, N. Tsuji and T. Sakai: *Acta Mater.*, 1999, **47**, 579-594.

17. R.Z. Valiev, R.K. Islamgaliev and I.V. Alexandrov: *Prog. Mater. Sci.*, 2000, **45**, 103-189.

18. K. Matsubara, Y. Miyahara, Z. Horita and T.G. Langdon: *Acta Mater.*, 2003, **51**, 3073-3084.

19. M. Kawasaki and T.G. Langdon: *J. Mater. Sci.*, 2007, **42**, 1782-1796.

20. R.B. Figueiredo and T.G. Langdon: *Adv. Eng. Mater.*, 2008, **10**, 37-40.

21. C. Michaelsen, K. Barmak and T. P. Weihs: *Phys. D*, 1997, **30**, 3167-3186.

22. A. K. Gupta, A. K. Jena and D. J. Lloyd: in 'Proceedings of the 6th International Conference on Aluminum Alloys,' 1998, 663-669, The Japan Institute of Light Metals, Tokyo, Japan.

23. M.J. Richardson and E.L. Charsley: in: 'Handbook of Thermal Analysis and Calorimetry', (Ed. M.E. Brown), Vol. 1, 547; 1998, Elsevier, Amsterdam. The Netherlands.

24. G. W. Smith, *Thermochim Acta*, 1997, **291**, 59-64.

25. A.K. Jena, A.K. Gupta and M.C. Chaturvedi: *Acta Metall.*, 1989, **37**, 885-895.

26. N. Gao, L. Davin, S. Wang, A. Cerezo and M. J. Starink: *Mater. Sci. Forum*, 2002, **396-402**, 923-928.

27. C. P. Tan and Y. B. Che Man: *Trend Food Sci. & Technol.*, 2002, **13**, 312-318.

28. D. Brabazon, D. J. Browne and A. J. Carr: *Mater. Sci. Eng.*, 2002, **A326**, 370-381.

29. M.J. Starink and P. van Mourik: *Mater. Sci. Eng.*, 1992, **A156**, 183-194.

30. M.J. Starink and P.J. Gregson: *Scripta Metall. Mater.*, 1995, **33**, 893-900.

31. M.J. Starink, A.J. Hobson, I. Sinclair and P.J. Gregson: *Mater. Sci. Eng*., 2000, **A289**, 130-142.

32. M.J. Starink, A.J. Hobson and P.J. Gregson: *Mater. Sci. Forum*, 2000, **331-337**, 1321-1326.

33. H. Jiang, Y. T. Zhu, D. P. Butt, I. V. Alexandrov and T. C. Lowe: *Mater. Sci. Eng.*, 2000, **A290**, 128-138.

34. J. T. Wang, W. Wei, Y. Zhang and G. Chen: in 'Ultrafine Grained Materials IV', (ed. Y. T. Zhu, T.G. Langdon, Z. Horita, M.J. Zehetbauer, S.L. Semiatin and T.C. Lowe), 89-96; 2006, TMS, Warrendale, PA, USA.

35. S. V. Dobatkin, J. A. Szpunar, A. P. Zhilyaev and A. A. Kuznetsov: in 'Ultrafine Grained Materials IV', (ed. Y. T. Zhu, T.G. Langdon, Z. Horita, M.J. Zehetbauer, S.L. Semiatin and T.C. Lowe), 401-406; 2006, TMS, Warrendale, PA, USA.

36. J. Gubicza, L. Balogh, R. J. Hellmig, Y. Estrin and T. Ungar: *Mater. Sci. Eng.*, 2005, **A400-401**, 334-338.

37. E. Schafler, G. Steiner, E. Korznikova, M. Kerber and M. J. Zehetbauer: *Mater. Sci. Eng*., 2005, **A410-411**, 169-173.

38. M. Furukawa, Y. Iwahashi, Z. Horita, M. Nemoto and T.G. Langdon: *Mater. Sci. Eng.*, 1998, **A257**, 328-332.

39. M. B. Beaver, D. L. Holt and A. L. Tichener: *Prog. Mater. Sci*., 1973, **17**, 5-177.

40. H. J. Wollenberger: in 'Physical Metallurgy', (Ed. R. W. Cahn and P. Haasen.), 1189-1221; 1983, North-Holland Publishing, Amsterdam, The Netherlands.

41. T. Ungar and A. Borbely: *Appl. Phys. Lett*., 1996, **69**, 3173-3175.

42. J. Wang, Y. Iwahashi, Z. Horita, M. Furukawa, M. Nemoto, R. Z. Valiev and T. G. Langdon: *Acta Mater.*, 1996, **44**, 2973-2982.

43. Y. H. Zhao, X. Z. Liao, Z. Jin, R. Z. Valiev and T. T. Zhu: *Acta Mater*., 2004, **52**, 4589-4599.

44. G. Angella, P. Bassani, A. Tuissi, D. Ripamonti and M. Vedani: *Mater. Sci. Forum*, 2006, **503-504**, 493-498.

45. W. J. Kim and J. Y. Wang: *Mater. Sci. Eng.*, 2007, **A464**, 23-27.

46. N. Gao, M. J. Starink, M. Furukawa, Z. Horita, C. Xu and T. G. Langdon: *Mater. Sci. Eng*., 2005, **A410-411**, 303-307.

47. N. Gao, M. J. Starink, M. Furukawa, Z. Horita, C. Xu and T. G. Langdon: *Mater. Sci. Forum*, 2006, **503-504**, 275-280.

48. M. J. Starink, N. Gao, M. Furukawa, Z. Horita, C. Xu and T. G. Langdon, *Rev. Adv. Mater. Sci.*, 2004, **7,** 1-12.

49. S. C. Wang and M. J. Starink: *Intl Mater. Rev.*, 2005, **50**, 193-215.

50. C. Xu, M. Furukawa, Z. Horita and T. G. Langdon: *Acta Mater*., 2003, **51**, 6139-6149.

51. C. Xu, M. Furukawa, Z. Horita and T. G. Langdon: *Acta Mater*., 2005, **53**, 749-758.

52. X. M. Li and M. J. Starink: *Mater. Sci. Technol*., 2001, **17**, 1324-1328.

53. N. Kamp, I. Sinclair and M. J. Starink: *Metall. Mater. Trans*., 2002, **A33**, 1125-1136.

54. M.J. Starink and X. M. Li: *Metall. Mater. Trans*., 2003, **A34**, 899-911.

55. M. Vedani, G. Angella, P. Bassani, D. Ripamonti and A. Tuissi: *J. Thermal Anal. and Calorim.*, 2007, **87,** 277-284.

56. J. Wang, Y. Iwahashi, Z. Horita, M. Furukawa, M. Nemoto, R. Z. Valiev and T. G. Langdon, *Acta Mater.*, 1996, **44**, 2973-2982.

57. M. A. Zaidi and T. Sheppard: *Metals Technol.*, 1984, **11**, 313-319.

58. E. Koken, J. D. Embury, T. R. Ramachandran and T. Malis: *Scripta Metall*., 1988, **22**, 99-103.

59. B. Mingler, O. B. Kulyasova, R. K. Islamgaliev, G. Korb, H. P. Karnthaler and M. J. Zehetbauer: *J. Mater. Sci.*, 2007, **42**, 1477-1482.

60. Z. Li, X. Cheng and Q. Shangguan: *Mater. Lett,,* 2005, **59**, 705-709.

61. X. Li and Y. Hsu: *Mater. Sci. Eng*., 1987, **A91**, 189-194.

62. X. Li and Y. Hsu: *Metallog.*, 1987, 20, 47-59.

63. A. Phillips, P.-W. Zhu and G. Edward: *Macromol.*, 2006, **39**, 5796-5803.

64. J. Karger-Kocis: 'Polypropylene', 57; 1999, Kluwer, Dordrecht, The Netherlands.

65. J. C. Viana, A. M. Cunha and N. Bilon: *Polymer,* 2002, **43**, 4185-4196.

66. Z. Y. Xia, H.-J. Sue and T. P. Rieker: *Macromol.*, 2000, **33**, 8746-8755.

67. C. G'Sell and A. Dahoun: *Mater. Sci. Eng*., 1994, **A175**, 4047-4050.

68. G. Sakai, Z. Horita and T. G. Langdon: *Mater. Sci. Eng*., 2005, **A393**, 344-351.

69. C. Xu, Z. Horita and T. G. Langdon: *Acta Mater.*, 2007, **55**, 203-212.

70. E. Korznikova, E. Schafler, G. Steiner and M. J. Zehetbauer: in 'Ultrafine Grained Materials IV', (ed. Y. T. Zhu, T.G. Langdon, Z. Horita, M.J. Zehetbauer, S.L. Semiatin and T.C. Lowe), 97-102; 2006, TMS, Warrendale, PA, USA.

71. D. Setman, M. Krystian and M. J. Zehetbauer: *Mater. Sci. Forum*, 2008, **584-586**, 355-360.

72. D. Setman, E. Schafler, E. Korznikova and M. J. Zehetbauer: *Mater. Sci. Eng*., 2008, **A493**, 116-122.

73. R. Wurschum, A. Kubler, S. Gruss, P. Acharwaechter, W. Frank, R. Z. Valiev, R. R. Mulyukov and H. E. Schaefer: *Annal. Chimie (Sci. Mater.)*, 1996, **21**, 471-482.

74. A. R. Yavari, W. J. Botta, C. A. D. Rodrigues, C. Cardoso and R. Z. Valiev, *Scripta Materialia*, 2002, **46**, 711-716.

75. N. Takata, K. Yamada, K, Ikeda, F. Yoshida, H. Nakashima and N. Tsuji: *Mater. Sci. Forum*, 2006, **503-504**, 919-924.

76. X. Huang, N. Tsuji, N. Hansen and Y. Minamino: *Mater. Sci. Eng.*, 2003, **A340**, 265-271.

77. N. Gao: *Mater. Sci. Forum*, 2008, **584-586**, 255-260.

78. L.F. Mondolfo: 'Aluminium Alloys: Structure and Properties', 1976, Butterworths. London. UK..

79. I. J. Polmear: 'Light Alloys, The Metallurgy of the Light Metals', 1995, Arnold, London. UK.

80. Y. Birol: *J. Mater. Sci.*, 2005, **40**, 6357-6361.

81. C. Y. Zahra and A.-M. Zahra: *Thermochim. Acta*, 1996, **276**, 161-174.

Table and Figure captions

Table 1. The enthalpies, ΔH, of different reactions during DSC annealing of UFG and CG Al-7075 samples.[43]

Fig. 1 Schematic cross-section of two types of differential scanning calorimeter. (a) heat flux DSC (figure supplied by Mettler-Toledo) and (b) power compensation DSC (figure supplied by Perkin-Elmer).[4]

Fig. 2 The DSC curves at a heating rate of 10°C/min for an Al-1.18% Cu-0.51% Mg-0.21% Mn alloy aged at 150°C.[26]

Fig. 3. The DSC scans at a 40°C/min heating rate for pure copper specimens deformed to different strain values through ECAP.[36]

Fig. 4. The stored energy determined by DSC at a heating rate of 10°C/min as a function of shear strain for deformation of copper samples using ECAP processing routes A, B_C and C.[37]

Fig. 5 The vacancy concentrations determined by DSC at a heating rate of 10°C/min and the residual electrical resistometry (RER) against the shear strain after ECAP processing for copper samples.[37]

Fig. 6. The DSC curves at a heating rate of 10°C/min for an Al-2024 alloy after ECAP.[47]

Fig. 7. The DSC curves at a heating rate of 10°C/min for an Al-7034 alloy after ECAP. [47]

Fig. 8. The DSC curves at a heating rate of 5 and 10°C/min for ECAP-processed UFG (solid lines) and CG (dotted lines) Al-7075 alloys.[43]

Fig. 9. The DSC curves at a heating rate of 20°C/min for two alloys investigated as a function of the number of ECAP passes. (a) Al-Mg-Si, (b) Al-Mg-Si-Sc.[44]

Fig. 10 The DSC curves at a heating rate of 10°C/min for Al-3%Mg alloy (a) after ECAP, (b) after cold-rolling to a reduction of 80% and (c) after cold-rolling and subsequent annealing for 3 h at 793 K.[56]

Fig. 11 The DSC curves at a heating rate of 30°C/min. as recorded from the initial AM60 (Mg–6% Al–0.13% Mn) sample and from samples after ECAP at different temperatures.[59]

Fig. 12. The DSC curves at a heating rate of 10°C/min for the TiNi alloy (a) before and (b) after 2 passes of ECAP.[60]

Fig. 13. The crystallinity index of isotactic polypropylene (iPP) at a heating rate of 10°C/min as a function of shear strain after ECAP.[63]

Fig. 14. The DSC curves at a heating rate of 40°C/min for (a) Cu samples processed by HPT for varying turns and (b) as-received Cu without HPT processing.[33]

Fig. 15. The Energy release and peak shift of the first exothermic peak at a heating rate of 40°C/min after HPT for Cu samples.[33]

Fig. 16. The DSC curves at a heating rate of 10°C/min for (a) 99.998% Ni and (b) 99.99% Ni, deformed by HPT.[70]

Fig. 17. (a) The dependence of dislocation and vacancy annealing temperature on applied shear strain and (b) the dependence of the stored energy of dislocations and vacancies, respectively, on the applied shear strain using a heating rate of 10°C/min for 99.998% Ni and 99.99% Ni after HPT.[70]

Fig. 18. The DSC curves at a heating rate of 5°C/min for hydrogenated undeformed Pd (solid line) and HPT Pd processed under an applied pressure of 8 GPa (dashed line).[71]

Fig. 19. The DSC curves for (a) melt-spun amorphous $Al_{90}Fe_5Nd_5$ and (b) HPT-consolidated disc material.[74]

Fig. 20. (a) The DSC curves at a heating rate of 40°C/min and (b) the Vickers hardness and released energy in 99.99% purity copper processed through various numbers of ARB cycles.[75]

ΔH (J/g)	Region I	Region II	Region III
UFG	7.04	−14.27	6.99
CG	6.98	−8.48	4.29

Table 1.

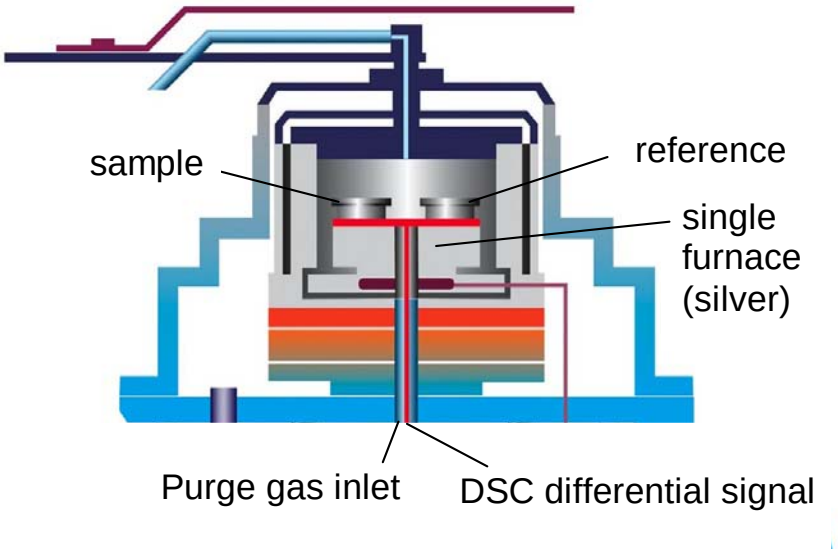
sample
reference
single
furnace
(silver)
Purge gas inlet
DSC differential signal

(a)

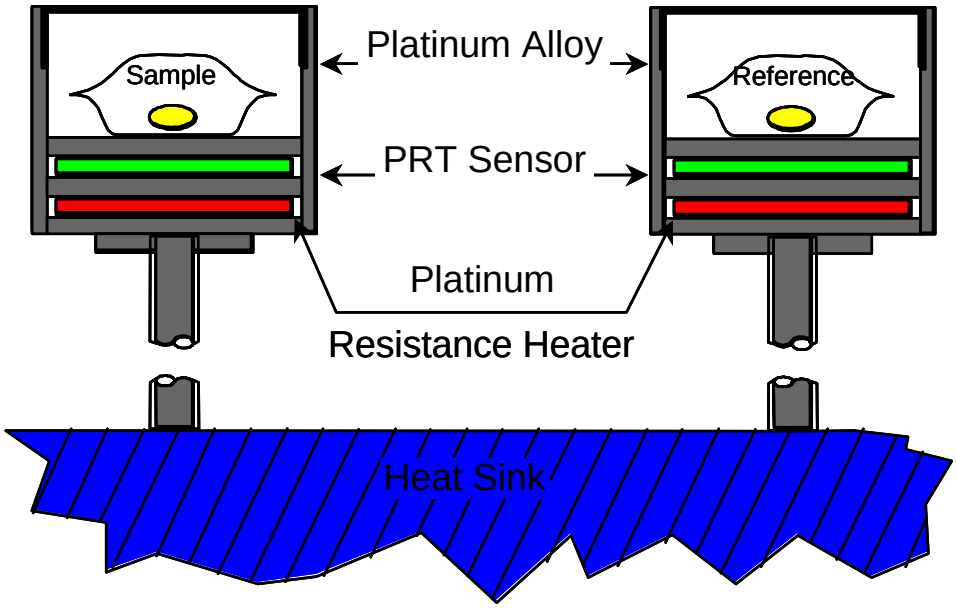
Sample
Platinum Alloy
Reference
PRT Sensor
Platinum
Resistance Heater
Heat Sink

(b)

Fig. 2

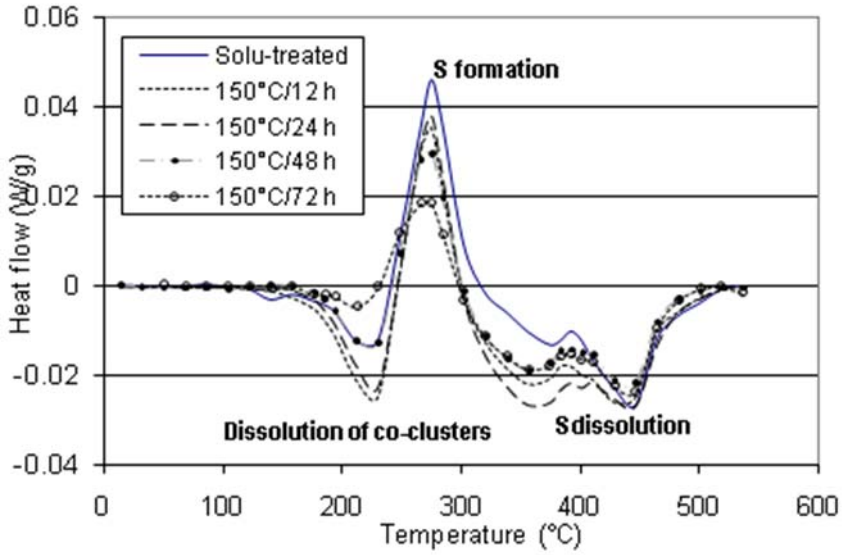
Solu-treated
150°C/12 h
150°C/24 h
150°C/48 h
150°C/72 h
S formation
Dissolution of co-clusters
S dissolution
Heat flow (W/g)
Temperature (°C)
0.06
0.04
0.02
0
-0.02
-0.04
0
100
200
300
400
500
600

Fig. 2

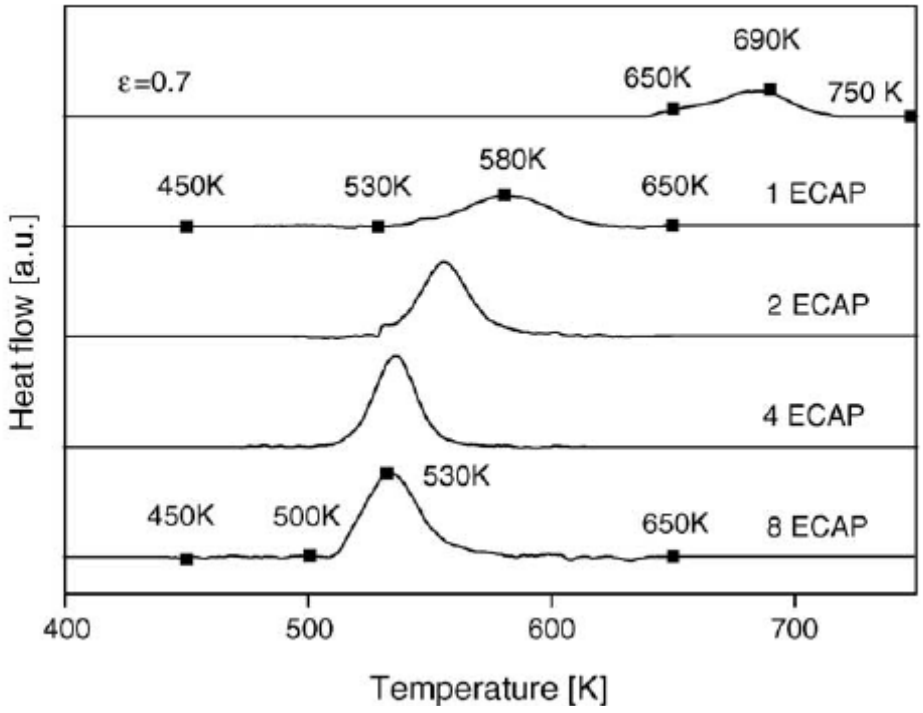
690K
ε=0.7
650K
750 K
580K
450K
530K
650K
1 ECAP
2 ECAP
4 ECAP
530K
450K
500K
650K
8 ECAP
Heat flow [a.u.]
400
500
600
700
Temperature [K]

Fig. 3.

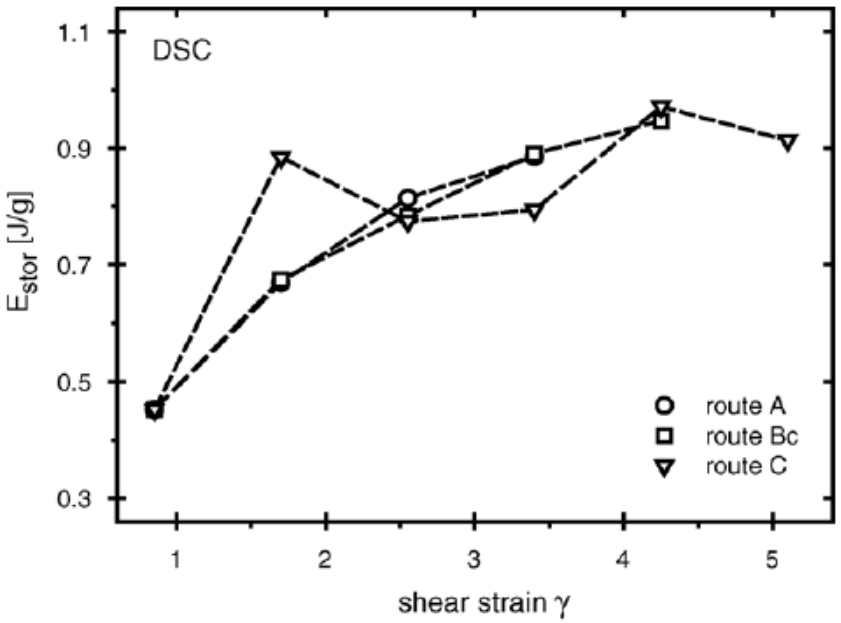
DSC
1.1
0.9
0.7
0.5
0.3
E_{stor} [J/g]
1
2
3
4
5
shear strain γ
route A
route Bc
route C

Fig. 4.

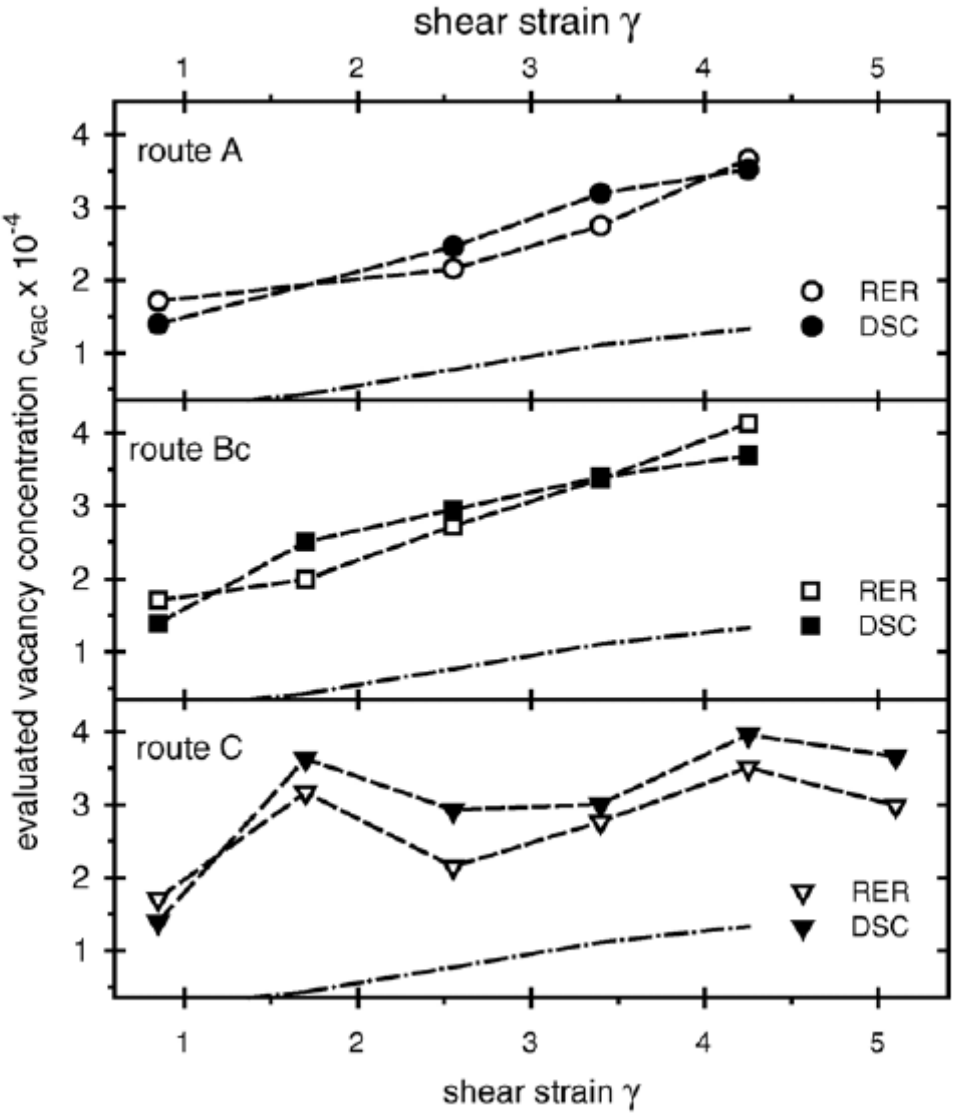
shear strain γ
1
2
3
4
5
route A
route Bc
route C
RER
DSC
evaluated vacancy concentration c_{vac} x 10^{-4}
shear strain γ

Fig. 5

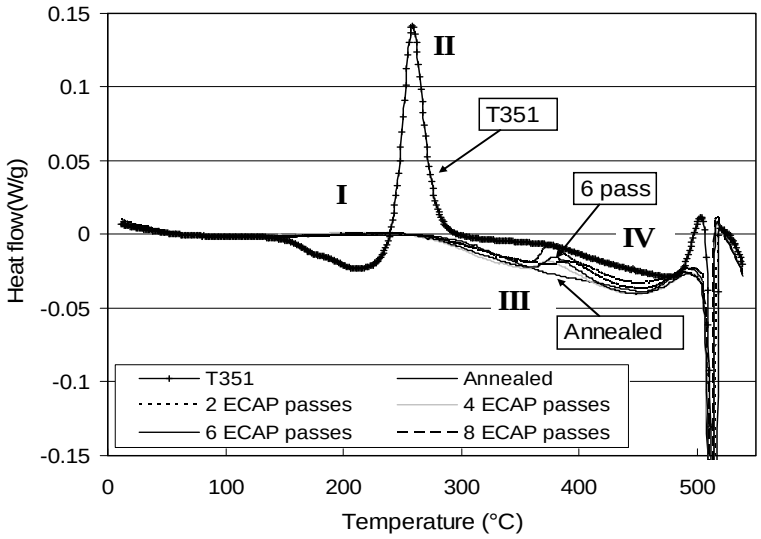
0.15
0.1
0.05
0
-0.05
-0.1
-0.15
Heat flow(W/g)
0
100
200
300
400
500
Temperature (°C)
I
II
III
IV
T351
6 pass
Annealed
T351
2 ECAP passes
6 ECAP passes
Annealed
4 ECAP passes
8 ECAP passes

Fig.6

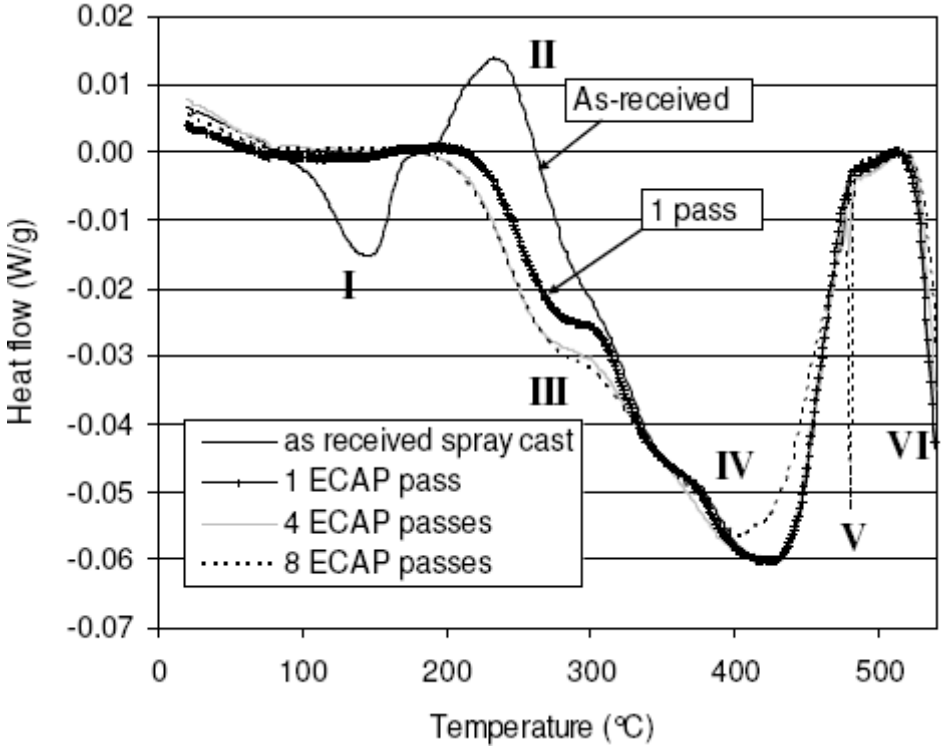
0.02
0.01
0.00
-0.01
-0.02
-0.03
-0.04
-0.05
-0.06
-0.07
Heat flow (W/g)
0
100
200
300
400
500
Temperature (°C)
I
II
III
IV
V
VI
As-received
1 pass
as received spray cast
1 ECAP pass
4 ECAP passes
8 ECAP passes

Fig. 7

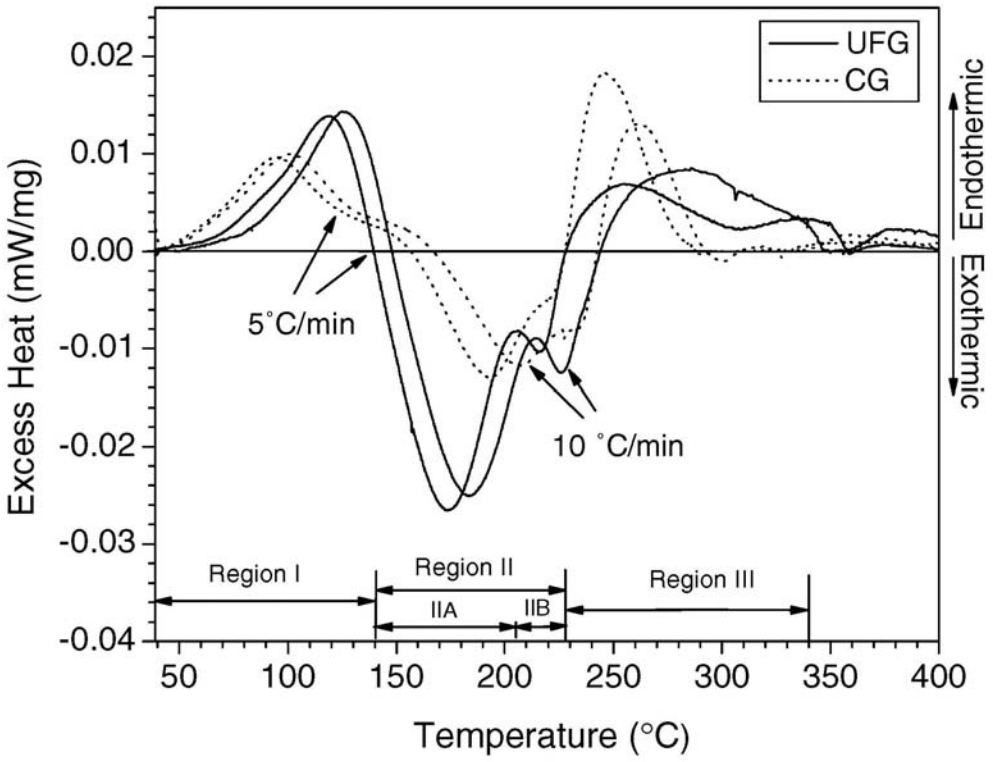
UFG
CG
Endothermic
Exothermic
Excess Heat (mW/mg)
0.02
0.01
0.00
-0.01
-0.02
-0.03
-0.04
5˚C/min
10 ˚C/min
Region I
Region II
IIA
IIB
Region III
50
100
150
200
250
300
350
400
Temperature (°C)

Fig. 8.

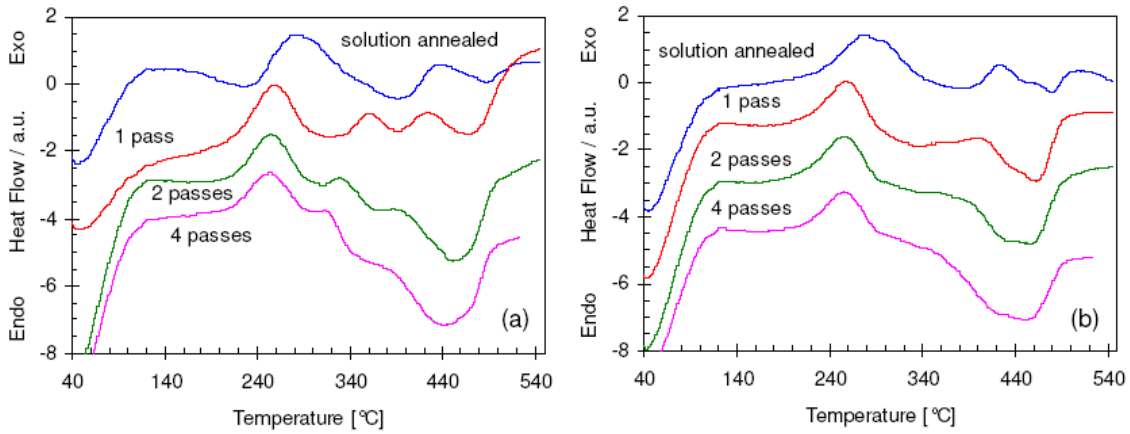
Exo
Heat Flow / a.u.
Endo
2
0
-2
-4
-6
-8
40
140
240
340
440
540
Temperature [°C]
solution annealed
1 pass
2 passes
4 passes
(a)
(b)

Fig. 9.

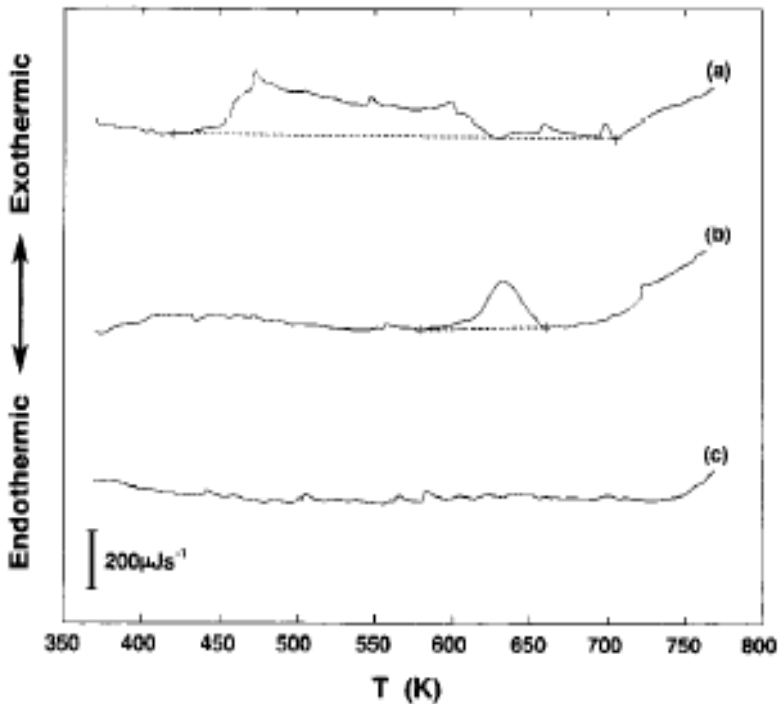
Exothermic
Endothermic
(a)
(b)
(c)
200μJs⁻¹
350
400
450
500
550
600
650
700
750
800
T (K)

Fig. 10.

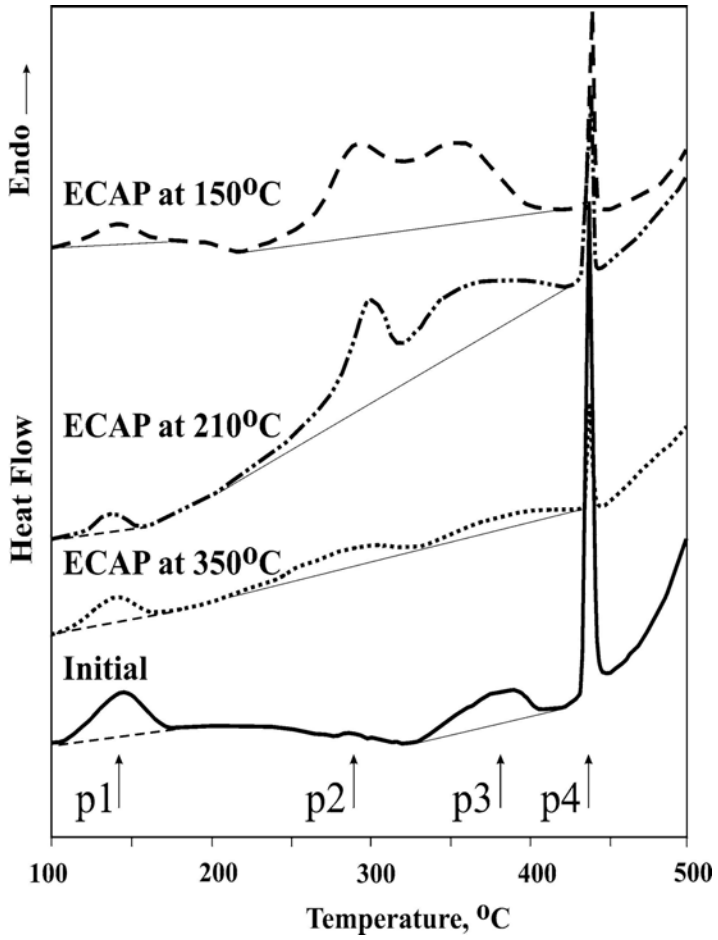
Endo ⟶
Heat Flow
ECAP at 150°C
ECAP at 210°C
ECAP at 350°C
Initial
p1
p2
p3
p4
100
200
300
400
500
Temperature, °C

Fig. 11.

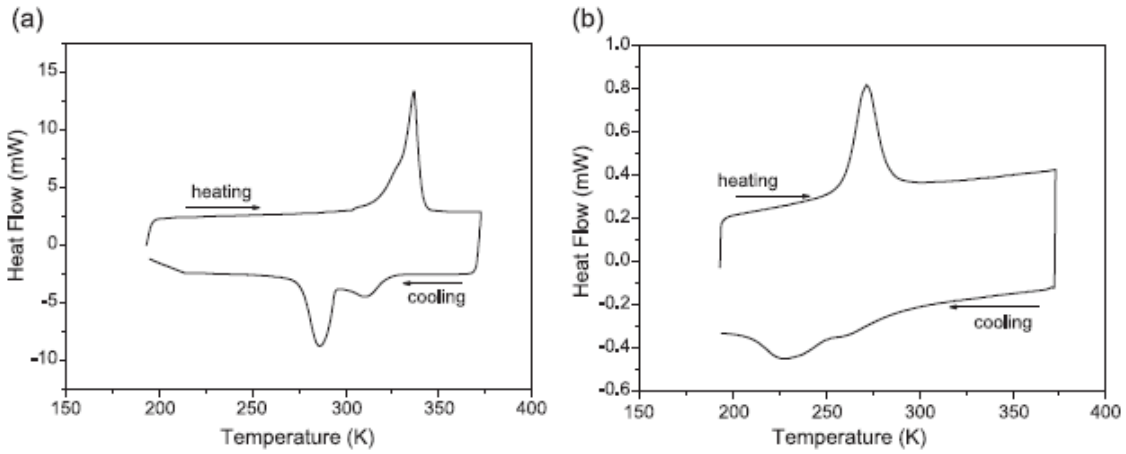
(a)
Heat Flow (mW)
15
10
5
0
-5
-10
heating
cooling
150
200
250
300
350
400
Temperature (K)
(b)
Heat Flow (mW)
1.0
0.8
0.6
0.4
0.2
0.0
-0.2
-0.4
-0.6
heating
cooling
150
200
250
300
350
400
Temperature (K)

Fig. 12.

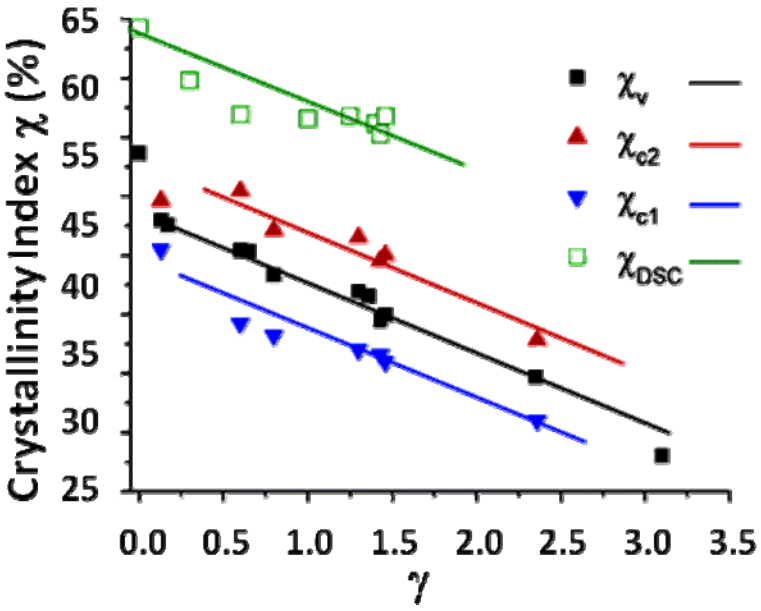
Crystallinity Index χ (%)
65
60
55
45
40
35
30
25
0.0
0.5
1.0
1.5
2.0
2.5
3.0
3.5
γ
χv
χc2
χc1
χDSC

Fig. 13.

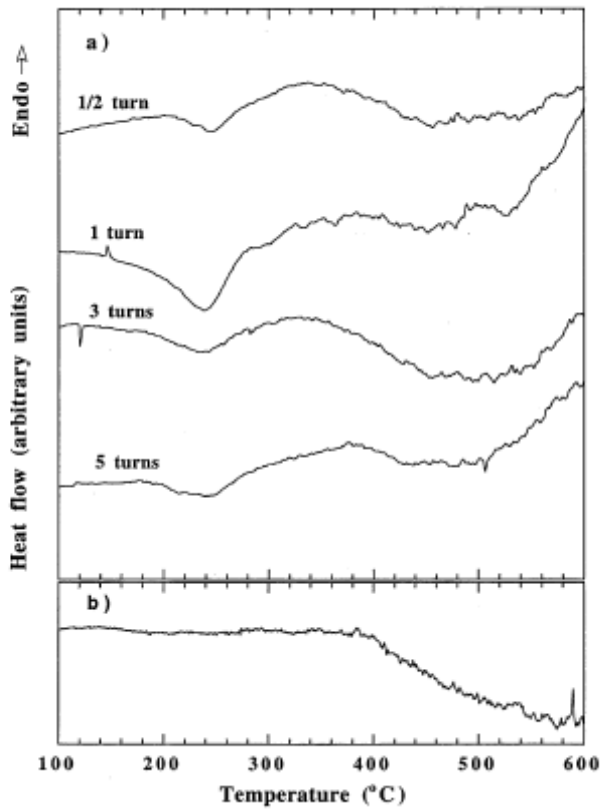
a)
1/2 turn
1 turn
3 turns
5 turns
b)
Endo
Heat flow (arbitrary units)
100
200
300
400
500
600
Temperature (°C)

Fig. 14.

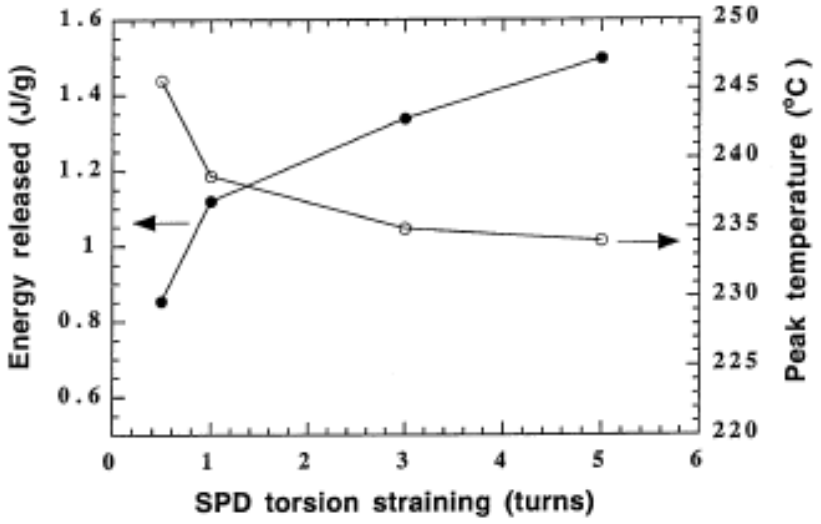
Energy released (J/g)
Peak temperature (°C)
SPD torsion straining (turns)
1.6
1.4
1.2
1
0.8
0.6
250
245
240
235
230
225
220
0
1
2
3
4
5
6

Fig. 15.

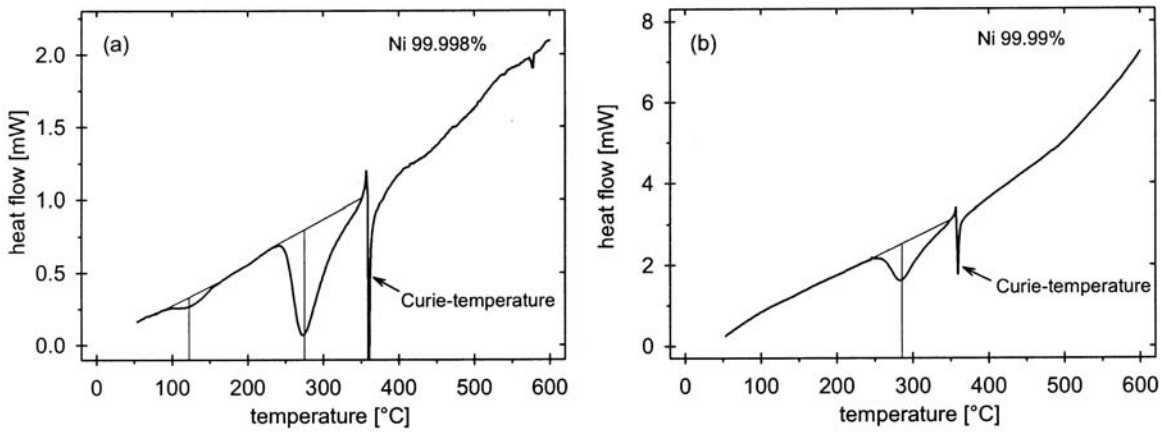
(a)
Ni 99.998%
heat flow [mW]
Curie-temperature
temperature [°C]
(b)
Ni 99.99%
heat flow [mW]
Curie-temperature
temperature [°C]

Fig. 16.

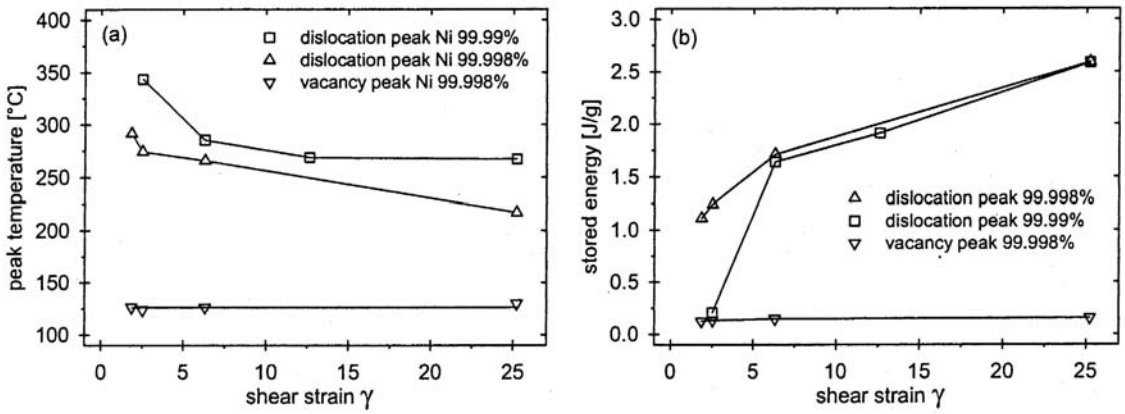
(a)
dislocation peak Ni 99.99%
dislocation peak Ni 99.998%
vacancy peak Ni 99.998%
peak temperature [°C]
shear strain γ
(b)
dislocation peak 99.998%
dislocation peak 99.99%
vacancy peak 99.998%
stored energy [J/g]
shear strain γ

Fig. 17.

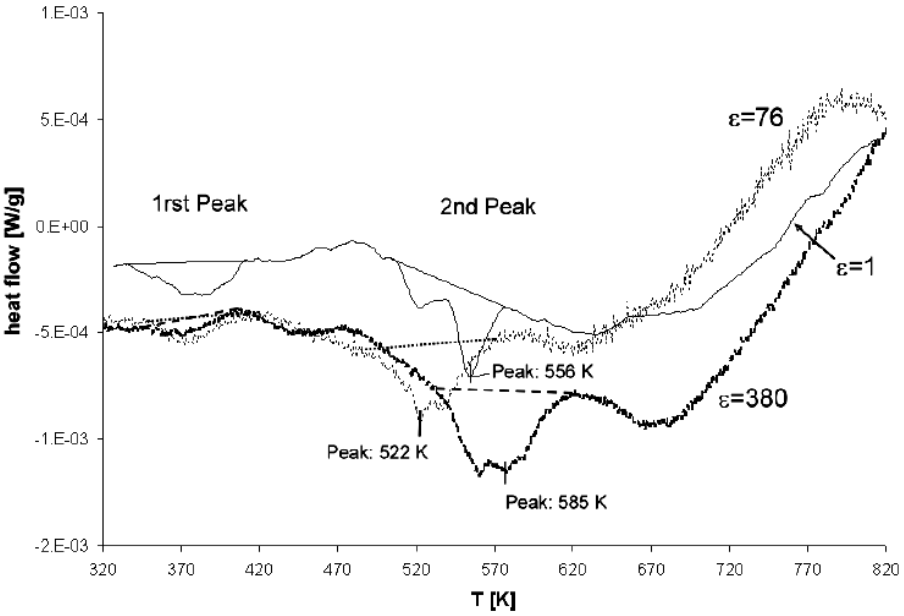
1.E-03
5.E-04
0.E+00
-5.E-04
-1.E-03
-2.E-03
heat flow [W/g]
320
370
420
470
520
570
620
670
720
770
820
T [K]
1rst Peak
2nd Peak
ε=76
ε=1
ε=380
Peak: 556 K
Peak: 522 K
Peak: 585 K

Fig. 18.

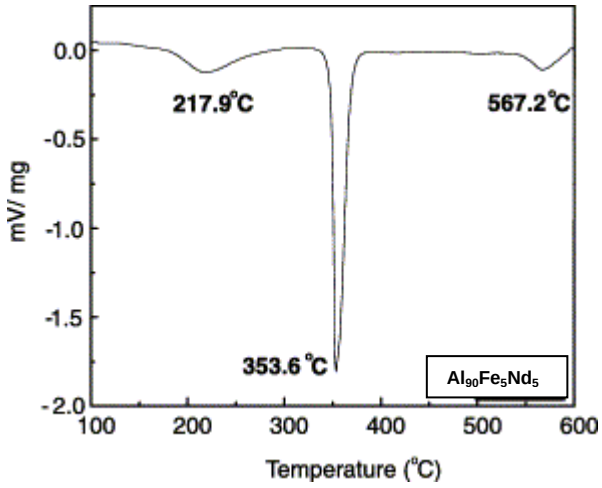
0.0
-0.5
-1.0
-1.5
-2.0
mV/ mg
217.9°C
567.2°C
353.6°C
Al90Fe5Nd5
100
200
300
400
500
600
Temperature (°C)

(a)

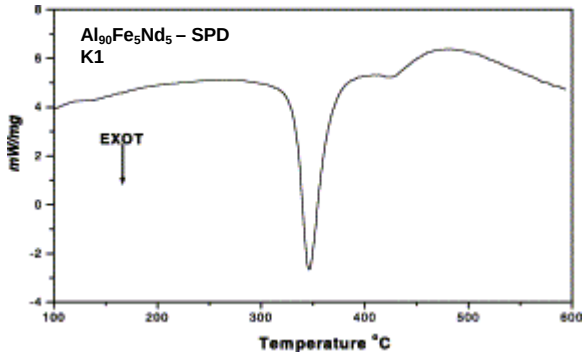
Al90Fe5Nd5 – SPD
K1
EXOT
mW/mg
Temperature °C

(b)

Fig. 19.

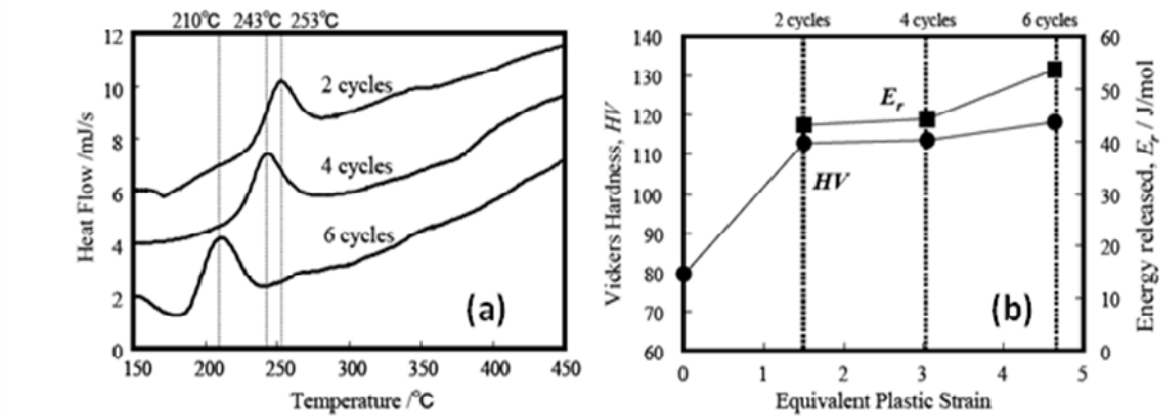
210℃ 243℃ 253℃
2 cycles
4 cycles
6 cycles
(a)
Heat Flow /mJ/s
Temperature /℃
2 cycles
4 cycles
6 cycles
E_r
HV
(b)
Vickers Hardness, HV
Energy released, E_r / J/mol
Equivalent Plastic Strain

Fig. 20